

Degrees of H2AX phosphorylation correlate with unique features of the intratumoral immune microenvironment in colorectal carcinomas

Enrico Berrino^{*,1,2, ID}, Sara Erika Bellomo¹, Maria Costanza Aquilano³, Marta Falcinelli⁴, Anita Chesta^{1, ID}, Emanuele Valtorta³, Daniela Zampieri¹, Gianluca Mauri^{3,5}, Giuseppe Sala^{3,5}, Silvia Marsoni^{4, ID}, Alberto Bardelli^{4,6}, Andrea Sartore-Bianchi^{3,5}, Salvatore Siena^{3,5}, Anna Sapino^{1,2}, Emanuela Bonoldi³, Fabrizio d'Adda di Fagnana^{4,7}, Caterina Marchiò^{*,1,2}

¹Pathology Unit, FPO-IRCCS Candiolo Cancer Institute, Candiolo, 10060 Italy

²Department of Medical Sciences, University of Turin, Turin, 10124 Italy

³Department of Hematology, Oncology, and Molecular Medicine, Niguarda Cancer Center, Grande Ospedale Metropolitano Niguarda, Milan, 20162 Italy

⁴IFOM ETS—The AIRC Institute of Molecular Oncology, Milan 20139, Italy

⁵Department of Oncology and Hemato-Oncology, Università degli Studi di Milano (La Statale), Milan, 20122 Italy

⁶Department of Oncology, Molecular Biotechnology Center, University of Torino, Torino 10126, Italy

⁷IGM and Institute of Molecular Genetics—CNR (National Research Council), Pavia, 27100 Italy

*Corresponding authors: Caterina Marchiò, Department of Medical Sciences, Università di Torino, FPO-IRCCS Candiolo Cancer Institute, Viale della Ricerca 7, 10060 Candiolo, Italy. E-mail: caterina.marchio@unito.it caterina.marchio@ircc.it; Enrico Berrino, FPO-IRCCS Candiolo Cancer Institute, Viale della Ricerca 7, 10060 Candiolo, Italy. E-mail: enrico.berrino@ircc.it.

Abstract

Background: The phosphorylated form of the histone H2AX (γ H2AX), a sensor of DNA double-strand breaks (DSB), can serve as a biomarker of DNA damage and therapy response. This study aimed to evaluate the association between γ H2AX expression and pathological, molecular, and immune features in colorectal cancer (CRC).

Patients and methods: Levels of γ H2AX were assessed by immunohistochemistry in a cohort of 198 CRCs, alongside immune-related markers (CD3 and CD8). A sub-cohort of 65 CRCs (26 γ H2AX⁻ and 39 γ H2AX⁺) underwent RNA extraction and gene expression profiling using the IO360 Nanostring Panel to infer immune cell composition. Overall survival data were analyzed for exploratory correlations.

Results: γ H2AX⁺ CRCs (155/198, 78%) were significantly associated with higher stage and tumor grade ($P < .01$). A lower γ H2AX prevalence was found in MMR-deficient tumors (64%) compared to MMR-proficient cases (81%, $P = .05$). γ H2AX⁺ tumors showed increased CD3⁺ cell infiltration in the overall population ($P = .038$) and in MMR-proficient CRCs ($P = .028$). Gene expression analysis revealed higher T-cell counts ($P < .01$) and reduced B-cell abundance ($P < .01$) in γ H2AX⁺ CRCs. Unsupervised clustering identified 3 immune subgroups with differential γ H2AX accumulation. Cluster #3, enriched in γ H2AX⁺ tumors, displayed increased CD8⁺ T-cells and conferred the best survival outcome.

Conclusion: Elevated γ H2AX expression correlates with MMR proficiency, aggressive histopathologic features, and a distinctive immune-active microenvironment in CRC. These findings may support γ H2AX as a marker of immune-modulated CRC subgroups with potential prognostic and therapeutic relevance.

Key words: γ H2Ax, MMR deficiently, MMR proficiency, colorectal cancer, immune infiltration

Received: November 5, 2025. Accepted: March 24, 2026

© The Author(s) 2026. Published by Oxford University Press.

This is an Open Access article distributed under the terms of the Creative Commons Attribution License (<https://creativecommons.org/licenses/by/4.0/>), which permits unrestricted reuse, distribution, and reproduction in any medium, provided the original work is properly cited.

Implications for Practice

Our findings identify γ H2AX as a novel biomarker defining a distinct subgroup of mismatch repair–proficient colorectal cancers (MMRp CRCs) with molecular and immune features resembling MMR-deficient/MSI tumors. MMRp/ γ H2AX⁺ lesions exhibit increased CD3⁺ and CD8⁺ T-cell infiltration and improved survival, suggesting a favorable immune-active phenotype. Incorporating γ H2AX evaluation into diagnostic workflows may enhance prognostic accuracy, refine patient stratification, and support personalized treatment approaches. γ H2AX may contribute to refining the immunobiological stratification of MSS CRCs thus broadening the potential applicability of immune-based therapies beyond MSI tumors.

Introduction

Genomic instability is essential for cancer initiation¹ and represents a major vulnerability.^{2,3} Several pharmacological treatments, from chemotherapy to PARP inhibitors, have been developed to exploit these genetic susceptibilities for cancer treatment.^{4–8} Several oncogenic events are associated with DNA damage and the concurrent activation of the DNA Damage Response (DDR) machinery.^{9–12} Among these DNA injuries, Double-Strand Breaks (DSBs), which are induced by genotoxic agents¹³ and ionizing radiation (IR),¹⁴ are repaired by homologous recombination (HR) or by non-homologous end joining (NHEJ) mechanisms.^{15–17} Upon DSB generation, the DDR protein kinases activation lead to the phosphorylation of the histone H2AX [phosphorylated(y)-H2AX] which spread across kilobases from the break.^{18,19} γ H2AX accumulation, organized in nuclear foci,²⁰ has been detected in several pre-malignant and malignant lesions,^{21–25} and recent findings defined a pivotal role in prevention of carcinogenesis.²⁶ In colorectal cancer (CRC) DSB accumulation is detrimental, however genomic instability represents a therapeutic vulnerability largely unexplored.²⁷ Studies evaluating the γ H2AX distribution in CRC are scarce. The largest study so far includes 92 CRCs stained by immunohistochemistry (IHC) and demonstrating that the higher the accumulation the more advanced stage and worse clinical outcome.²⁸ However, poor correlations could be performed due to the absence of the mismatch repair (MMR) status, a major carcinogenetic driver in CRC. MMR deficiency (MMRd) leads to peculiar phenotypical features, able to modulate both cancer cells and tumor microenvironment.²⁹ MMRd tumors usually show meaningful immune infiltration, especially by T-cells, due to an elevated repertoire of neoantigens associated to high tumor mutational burden.^{30–32} In this scenario, less is known about γ H2AX accumulation and the immune infiltrate. A mild correlation of γ H2AX with CD3 and CD4 expression was reported in early-stage lung cancers,³³ and similarly a slight but not significant correlation with TILs was detected in 76 metaplastic breast carcinomas.³⁴

Here, we report on γ H2AX accumulation in a sequential cohort of 200 CRCs, evaluating its relationship with several pathological features, with a focus on MMR status and immune microenvironment.

Material and methods

Patient cohort

We collected an unselected sequential cohort of therapy-naïve 200 CRCs (2018–2020) at Grande Ospedale Metropolitano

Niguarda, Milan, Italy, within the frame of the AlfaOmega Master Observational Trial (Ethical Committee of Grande Ospedale Metropolitano Niguarda, #145-07042020; NCT04120935 and NCT05101382).³⁵ This study was conducted in accordance with the Declaration of Helsinki and the International Conference on Harmonisation and Good Clinical Practice guidelines.

The following clinical data were recorded: sex, age at diagnosis, type of treatment, stage, side, *RAS/BRAF* status, occurrence of relapse, and last follow-up or death. Full histopathological parameters were recorded, including results for MSH2/MSH6/MLH1/PMS2 expression by IHC.³

Immunohistochemistry

Five micron-thick formalin fixed paraffin embedded (FFPE) sections were stained with the anti-gamma H2A.X antibody (phospho S139, 1:1000 diluted, ab11174) on the Dako Omnis instrument (Dako-Agilent, USA). Two pathologists assessed the accumulation of γ H2AX reporting both nuclear intensity of staining and percentage of positive cells into a 4-tier scoring system, from 0 (absent staining) to 3 (strong staining) (Figure 1A).

Samples were also tested for CD3 (Polyclonal, Ready-to-Use, Dako-Agilent) and CD8 expression (Clone C8/144B, Ready-to-Use, Dako-Agilent) on the Dako Omnis instrument (Dako-Agilent). These markers were used to quantify the tumor infiltrating lymphocytes (TILs), including geographic distribution of the markers and the overall expression within the tumor area.

RNA extraction

RNA-based analyses were performed on 85 CRCs selected for adequate tumor content, optimal RNA quality, and representativeness of γ H2AX expression. Three 8- μ m sections were mesodissected for RNA extraction using the Maxwell FFPE RSC kit (Promega, USA). RNA was quantified by Qubit (Thermo Fisher Scientific, USA), and analyzed for integrity and fragment distribution using the High Sensitivity RNA ScreenTape assay (RIN and DV200 metrics) on the Agilent 4150 TapeStation (Agilent, USA).

Gene expression analysis

The gene expression of 770 genes was assayed by the PanCancer IO 360 panel, a targeted gene expression profiling (GEP) approach (NanoString Technologies, USA). Briefly, 500 ng of RNA were subjected to an overnight incubation at 56 °C (for 14 hours) with pre-designed oligo probes to capture the targeted genes. Exploiting the NanoString nPrep Station we purified samples, and the NanoString nCounter instrument read the

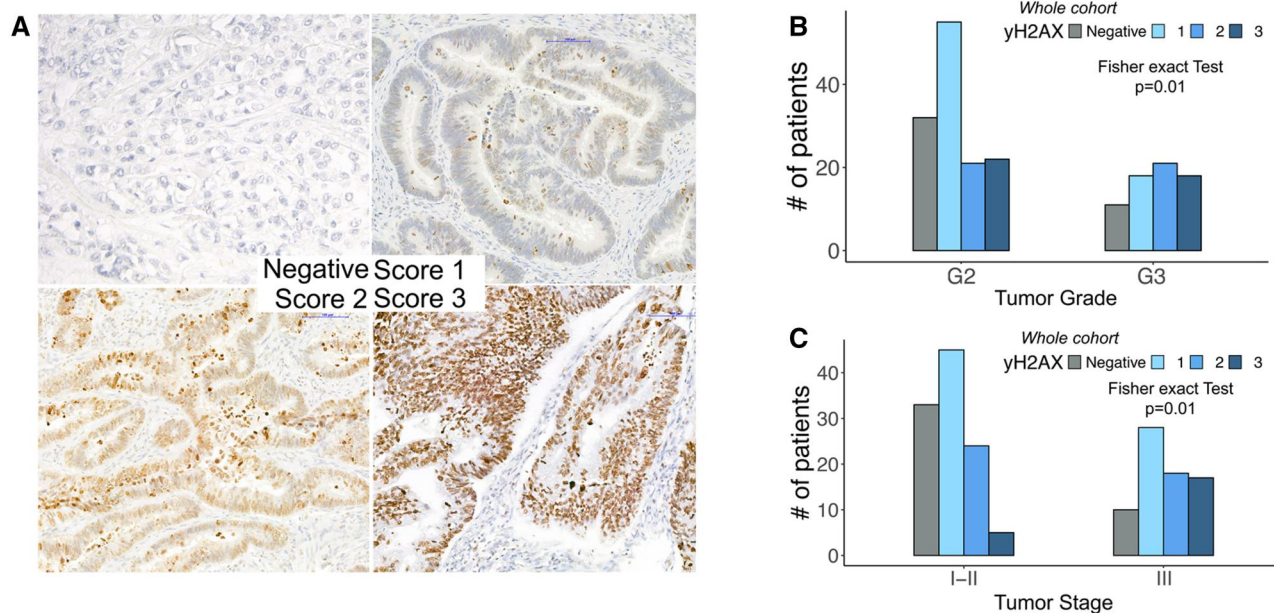


Figure 1. yH2AX accumulation in the CRC cohort. (A) Example of increasing yH2AX staining in CRCs, from negative to score 3. (B) Barplot and contingency table of yH2AX score in differentiated (G2) vs dedifferentiated G3 CRCs revealed a differential yH2AX accumulation in respect to the tumor grade. (C) Barplot and contingency table of yH2AX score in earlier (stage I-II) vs advanced (stage III-) G3 CRCs revealed a differential yH2AX accumulation in respect to the tumor staging.

associated fluorescence (NanoString Technologies). Raw results were elaborated using the nSolver Software (NanoString Technologies), exploiting the nSolver Advanced Analyses package.³⁵ Twenty samples did not meet QC criteria, resulting in a final analytical cohort of 65 cases. Volcano plots for the differential gene expression (DGE) among the yH2AX groups were generated using the ggplot R package using $P < .0001$ and FoldChange (Fc) expression > 1.5 as cutoffs for significance. Raw and relative cell type score as well as the pathways scores were used to cluster the 65 patients using the *k*-means algorithm implemented in the ComplexHeatmap R package (clustering method: “ward.D,” clustering distance: “Euclidean”). We selected the best *k* using the silhouette score calculated with the “cluster” R package (v.2.1.6).

Statistical analysis

Statistical analyses were performed using R software (v.4.0.3). For the correlative analysis, yH2AX accumulation was used to stratify the entire cohort for the IHC Scores (0, 1, 2, 3) and for the IHC Value (Negative vs Positive). We used the chi-square test for correlative analyses between yH2AX groups and clinico-pathological features, the t-test was applied for distribution comparison of both the CD8⁺ and CD3⁺ IHC expression values (%) and the RNA-inferred scores (both pathway and cell type scores). For survival analyses, Overall Survival (OS, calculated as the time from diagnosis to death or last follow-up date) was evaluated by the Kaplan–Meier method and analyzed with the log-rank test and by univariate and multivariate Cox Proportional Hazard Model with the *r* packages *survival* and *finalfit*. *P*-values with false discovery rate correction (FDR) < 0.05 were considered as statistically significant.

Results

yH2Ax accumulation across CRCs and correlation with clinico-pathological features

We successfully assessed yH2Ax protein accumulation by IHC in 198/200 CRC. In 2 cases pre-analytical issues led to non-uniform staining throughout the sections (cases excluded from further evaluation).

Forty-three of 198 tumors (22%) were classified as score 0, whereas 73/198 (38%) showed low expression (score 1), 42/198 (21%) intermediate expression (score 2), and 37/198 (19%) strong accumulation (score 3) (Figure 1A). By the dichotomous classifier [grouping tumors as γ H2AX-negative (score 0) vs positive (score 1–3)], 43/198 CRCs (22%) were γ H2AX negative, while 155/198 (78%) showed detectable expression.

We then cross-correlated both IHC classifier and scores with all the main clinico-pathological features (Table S1, summarized in Table S2). We identified few associations between yH2AX accumulation and patient characteristics: neither the primary site (colon vs rectum) nor the tumor side (left vs right) were significantly associated with differential yH2AX accumulation (Table S3). However, contingency table with Fisher’s exact test showed that positivity for yH2AX was more pronounced in the advanced stage (III-IV) compared to the early CRCs ($P = .03$ for yH2AX Value and $P < .01$ for yH2AX Score, Figure 1B). Moreover, the accumulation of yH2AX was not related with histology (adenocarcinoma not otherwise specified vs mucinous carcinomas) or with the percentage of mucinous component. More differentiated tumors (G2) showed a higher, yet not statistically significant, proportion of γ H2AX-negative cases than poorly differentiated tumors (G3) using the dichotomous classifier (25% vs 16%, $P = .17$; Table 1).

Table 1. Correlation between γ H2AX expression and clinico-pathological features.

γ H2AX value crosstabs ($n = 198$)		Negative	Positive	<i>P</i>
Histology	ADK	33	10	.4
	Mucinous	127	28	
Mucinous component (%)	ADK	19	90	.25
	0			
	1-25			
	26-49			
Tumor grade	50-100	10	28	.17
	G2	32	98	
	G3	11	57	
Vascular invasion	Absent	35	116	.37
	Present	8	39	
Lympho-vascular invasion	Absent	30	87	.1
	Present	13	68	
Tumor budding	Bd0	5	13	.05
	Bd1	32	86	
	Bd2	2	20	
	Bd3	4	35	
MMR status	MMRd	10	18	.05
	MMRp	33	137	
Primary site	Colon	38	141	.61
	Rectum	5	14	
Colon side	Right	26	85	.7
	Left	12	52	
Stage	I-II	33	92	.03
	III	10	63	

The full ordinal IHC score (0–3) revealed a significant distribution difference across tumor grades (Figure 1B, $P < .01$; Table S3). γ H2AX negative lesions showed a reduced tumor budding (Bd0-1:86%) compared to γ H2AX positive CRCs, characterized by a 36% of tumors with Bd2-3 ($P = .05$, Table 1).

Overall, γ H2AX accumulation was broadly distributed across CRCs and associated with aggressive features (grade, stage, and budding), rather than location or histological subtype.

Correlation between γ H2AX accumulation, MMR status and IHC biomarkers of immune cell infiltration

Based on the assessment of MLH1/PMS2/MSH2/MSH6 expression our cohort was composed of 172/198 (86%) MMR proficient (MMRp) and 28 MMR deficient (MMRd) CRCs (14%). We investigated whether MMR status could be related with differential γ H2AX accumulation. To avoid hyper-stratification of the small MMRd cohort (28 CRCs, distributed in 10 γ H2AX negative, 8 with score 1, 5 with score 2 and 5 with score 3), we used the dichotomous separation into positive vs negative. We identified a lower prevalence of γ H2AX positive CRC (18/28, 64%) in the MMRd lesions, compared to the MMRp CRCs (137/170, 81%, $P = .05$, Figure 2A and Table 1). All the MMRd CRCs were right-sided

(26/28), thus precluding assessment of the correlation of the γ H2AX staining related to side of primary tumor origin. No differences in terms of site (colon vs rectum) nor for colon tumor side (left vs right) were identified for the γ H2AX accumulation in the MMRp cohort, in which the G2 CRCs confirmed to be less prone to the accumulation of this biomarker compared to poorly differentiated CRCs (G3 $P = .02$).

Subsequently, we wondered if immune infiltration could be associated with degrees of γ H2AX accumulation. We started from a simple IHC-based approach assessing CD3- and CD8- positive T cells. In the 198 CRCs successfully stained with the γ H2AX antibody a mean of CD3⁺ and CD8⁺ positivity of 14.5% and 5.3%, respectively, was observed. We then compared the distribution of immune markers within the γ H2AX classes. A trend of reduced CD3⁺ staining was identified in the γ H2AX negative CRCs, compared to the γ H2AX positive CRCs [Negative: 6.0% (9.0-16.8), 1: 12.6% (12.3-17.8), 2: 13.0% (11.5-18.5), 3: 12.5% (11.9-20.3)]. When using the IHC classifier (Negative vs Positive), we identified a significant increase of CD3⁺ cells in the γ H2AX positive tumors (6.0 (9.0-16.8) vs 12.5 (13.4-17.2), $P = .038$, Figure 2B). No significant correlations between CD8 and γ H2AX expression were observed (Table S4).

We next assessed the distribution of the immune markers in the context of the MMR status: beside a superimposable amount of CD3⁺ cells, MMRd tumors exhibited a significantly higher CD8⁺ cells compared to the MMRp CRCs (6.6% (4.9-15.2) vs 2.5% (3.6-5.6), $P = .002$, Figure 2C). This feature prompted us to consider the γ H2AX-immune marker association separately for MMRd and the MMRp cases. In the MMRd population ($n = 28$), we were not able to confirm the increase of CD3⁺ cells in the γ H2AX positive lesions ($P = .11$), and no differences in CD8 expression were identified ($P = .6$). Conversely, γ H2AX-high, MMRp tumors showed a significantly higher CD3 expression ($P = .01$, Figure 2D), whereas statistical significance was not reached when analyzing CD8 ($P = .4$, Table S4).

Taken together, these data show that the association between γ H2AX and T-cell infiltration is mainly observed in MMRp tumors, with increased CD3+ T-cell levels in γ H2AX-positive cases.

Gene-expression based immune cell count and pathway scoring in the different levels of γ H2AX accumulation

Since the simple CD3/CD8 IHC assay revealed a significant correlation of different levels of γ H2AX accumulation with the amount of CD3⁺ positive cell (a T cell universal biomarker), but no differences in terms of CD8⁺ positive cell distribution were observed, we aimed at exploring the composition of the immune infiltrate of CRCs. We exploited a GEP targeted approach on 65 representative samples (26 negative and 39 positive for γ H2AX) in terms of MMR features and CD3/CD8 expression (summarized in Table S5). In addition to the immune cell inference scores, we assessed CD3 complex transcripts (*CD3D*, *CD3E*, *CD3G*) from the NanoString panel. *CD3D* and *CD3E* were significantly upregulated in γ H2AX-positive tumors ($P = .022$ and $P = .001$), while *CD3G* showed no difference ($P = .76$). These results are consistent with CD3+ IHC and support increased T-cell abundance in γ H2AX-positive CRCs (Figure S1). We inferred the immune cell

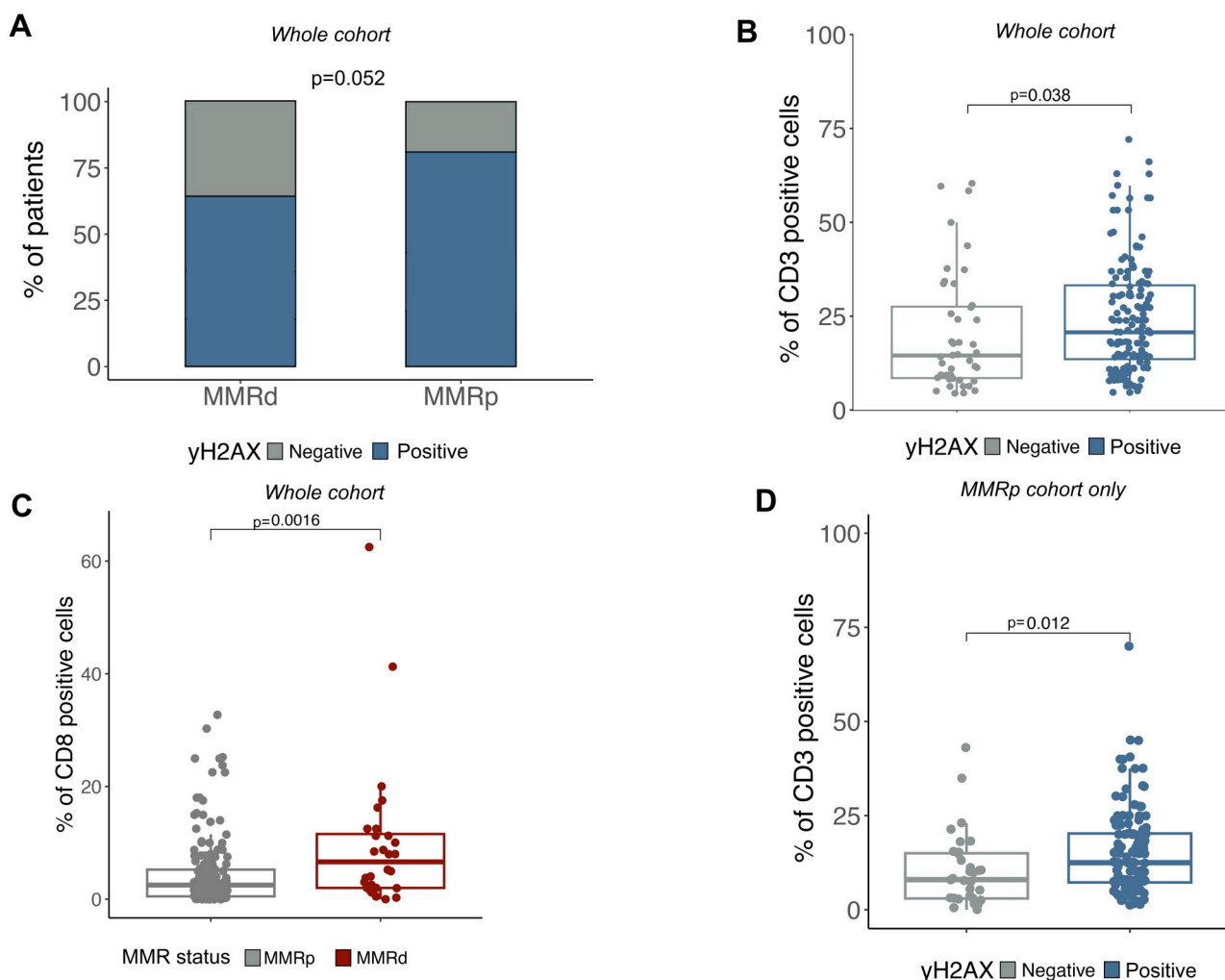


Figure 2. Correlation between yH2AX accumulation and CRC features. (A) Stacked barplot reporting the percentage of each yH2AX group and the MMR status. (B) Boxplot the CD3 positivity and the yH2AX score-based groups. (C) Boxplot the CD8 positivity and the MMR status-based groups. (D) Boxplot the CD3 positivity and the yH2AX value-based groups in the MMR proficient cohort.

count from transcriptomic data, generating for each patient a score defining the quantity of each immune cell type (raw count) and a score representing the ratio between each single cell type and the inferred total TILs (relative count). The distribution of the raw and relative counts is reported in Figure 3A-B. First, when we compared the distribution of raw and relative counts, yH2AX positive CRCs showed a higher count of relative T-Cells (Table 2, $P < .01$), in contrast with a lower abundance for relative B-Cells (Table 2, $P < .01$) compared to the yH2AX negative tumors. No other correlations were observed.

Therefore, we asked if a composite signature rather than a cell type score could be more relevant to dissect potential correlations with yH2Ax accumulation. To this end, we applied unsupervised clustering on both raw and relative cell count on the entire cohort. In terms of raw count, k-mean clustering (optimal $k=2$, Figure S2A-B) stratified tumors for the quantity of immune infiltration, identifying a group of “hot” CRCs (Cluster II), enriched for all immune cell types, and mainly correlated with the MMR status (16/18, 89% belong to the cluster II, $P < .01$, Figure S2C). No associations between the yH2AX status and these clusters were identified, considering both the entire

cohort and the CRCs stratified according to the MMR status (Figure S2D-F).

We next explored the ability of the relative cell count to group the CRCs. By this analysis we identified 3 groups with a trend of enrichment for yH2AX accumulation in cluster #2 and #3 ($P = .12$, Figure S3A-C). When we applied the same approach to MMRd and MMRp CRCs separately, the latter cohort reached a significant stratification of yH2AX accumulation (best $k=3$, $P = .02$, Figure 3C) in contrast with the k-mean clustering for the MMRd cohort (best $k=2$, $P = .32$; Figure S3D).

Figure 3C reports the clusters for the MMRp cohort: cluster #1 was mainly enriched of yH2AX negative lesions (9/13, 70%), whereas the other 2 clusters, with a different pattern of relative cell type composition, showed a larger number of yH2AX positive CRCs (14/17, 82% and 12/18, 67% for cluster#2 and 3, respectively). The relative-score clusters did not overlap with the hot/cold classification based on raw counts, with no association in MMRp tumors ($\chi^2 P = .78$; Figure 3D). Overall, while raw immune abundance reflected MMR status, relative composition better stratified yH2AX within MMRp CRCs.

Next, we applied distribution test to characterize the IHC based score, the raw and the relative cell count within the 3

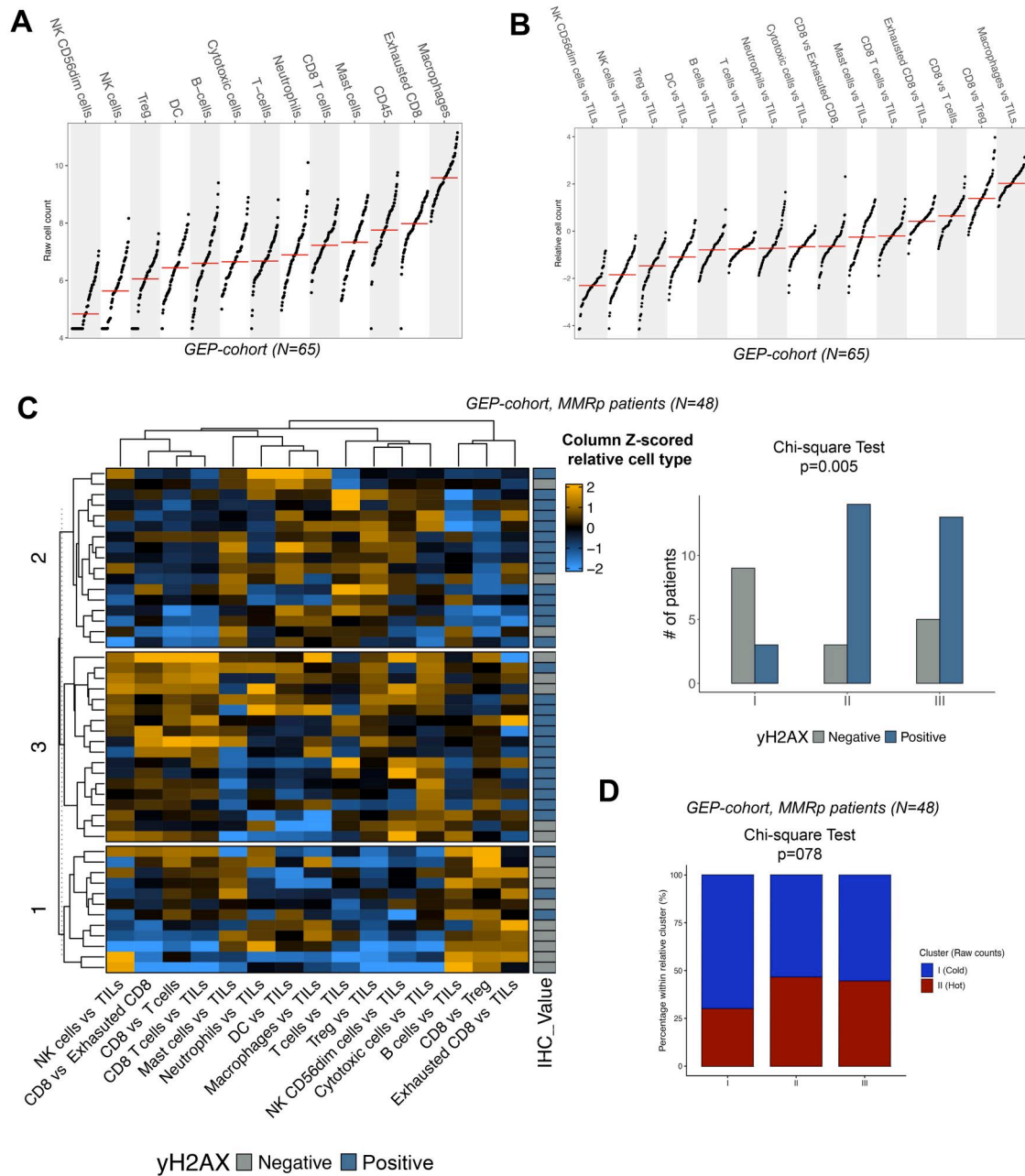


Figure 3. Gene-expression based immune cell type scores and the correlation with the yH2AX accumulation. (A) Distribution of the raw immune cell type count in the CRC cohort. (B) Distribution of the relative immune cell type count in the CRC cohort. (C) *K*-mean clustering of relative immune cell count in the MMR proficient CRC cohort, annotated for the yH2AX value with the barplot reporting the differential distribution of yH2AX accumulation within the *k*-mean identified clusters. (D) Stacked barplot reporting the differential distribution of raw immune cell type clusters (“hot” and “cold”) within relative immune cell type clusters.

clusters. The *P*-value heatmap reports the significant results in Figure 4A. Cluster #1 showed a reduced expression of CD3 marker compared to the other 2 groups ($P < .05$ for both). In the same cluster, we observed a B-cell enrichment, for both raw and relative counts, in line with the yH2AX negative predominant composition. The same group was enriched also in exhausted CD8 T (Figure 4B) but depleted in regulatory T cells (Treg). Cluster #2 was characterized by a higher infiltration of dendritic cells (DC, both raw and relative), and by a higher relative quantity of T-cells/total TILs (Figure 4C). Finally, cluster#3 showed a

clear increase in CD8 T-cells in the RNA-based test, for both the total and all the relative comparisons (vs TILs and vs all the other T cell types Figure 4D).

Through a differential expression analysis on the 770 analyzed genes, we identified few genes differentially expressed between cluster#2 and #3, whereas several genes varied between cluster#1 and the others (Figure S4). Finally, through the pathway score assessment, we evaluated the most differentially activated signaling pathway within the clusters. Although an unsupervised analysis did not identify combined signaling signatures able to

Table 2. Correlation yH2Ax expression and CD3 and CD8 positivity in the RNA-analysed cohort.

Cohort	yH2Ax negative vs positive	Wicox-test (P-value)
All (n = 65)	B cells/TILs*	.01
	T cells/TILs*	<.01
MMRd only (n = 18)	B cells/Tal*	.3
	T cells/TILs*	.07
MMRp only (n = 47)	B cells/TILs*	.01
	T cells/TILs*	.01

reconstruct the immune-clusters, distribution test showed some pathways specific for each subgroup. As reported in [Figure 4E](#), cluster#1 was clearly enriched for Notch activation compared to the 2 yH2AX positive clusters. Cluster #3 displayed a higher activation of the DNA-damage repair pathway, cluster#2 was characterized by a significant enrichment of costimulatory signaling ([Figure 4F-G](#)). [Figure S5](#) reports the DDR genes differentially expressed between the 2 clusters: cluster#3 was enriched for *BRCA1/2*, *RAD51C*, *FANCA*, and *POLD1*.

Collectively, these findings demonstrate that γ H2AX-positive MMRp tumors segregate into biologically distinct immune configurations, characterized by either priming/costimulatory or cytotoxic/DDR-associated axes.

Explorative correlations between yH2AX accumulation and clinical outcomes

We collected OS data for all the patients; we excluded 19 patients since immediately metastasized after surgery. By applying an explorative Univariate Cox Proportional Hazard Model, adjuvant therapy emerged as the major stratifier of the cohort (HR: 0.29, range: 0.14-0.57, $P < .001$). Multivariate analysis ([Table S6](#), [Figure S6](#)) reported a poor prognostic role for higher tumor grade [HR: 1.86 (1.00-3.47), $P = .049$], non-rectal localization (HR: 0.26, range: 0.08-0.80, $P = .019$) and a trend of lower OS for MSS lesions (HR: 2.35, range: 0.96-5.73, $P = .061$). In this scenario, yH2AX accumulation did not stratify the cohort for the survival, with forest plot ([Figure S6](#)) and Kaplan Meier plot ([Figure S7](#)) showing a non-significant, highly variable HR of 1.45 for yH2AX-positive CRCs. When focusing on MMRp lesions, the multivariate analysis returned significance only for tumor grade (HR: 2.59, range 1.48-4.54, $P = .001$), with adjuvant treatment not associated with a differential OS ([Table S7](#)).

Next, we tested if the clusters based on the relative immune infiltration related to the yH2AX accumulation identified in the MMRp lesions was associated with OS. Multivariate analysis showed that cluster #3 (yH2AX positive) represented a clear-cut favorable factor compared to cluster #1, mainly composed by yH2AX negative ([Table S8](#) and [Figure S8](#)). Kaplan-Meier ([Figure 5](#)) confirmed this trend, with cluster #2 showing an intermediate OS.

Overall, γ H2AX accumulation alone did not significantly stratify survival; however, immune-based clustering within MMRp tumors identified subgroups with distinct prognostic trajectories.

Discussion

In the era of the preclinical models several studies have reported on the exciting role of DNA damage and repair, defining several new predictive or prognostic cancer biomarkers.³⁶⁻³⁸ However, their validation often failed upon translation to real-world cancer cohorts.^{39,40} Here, we assessed yH2AX accumulation in a consecutive cohort of early CRCs. yH2AX positive lesions exhibited features of aggressiveness (higher tumor grade and stage) and yH2AX lack of expression was more frequently associated with MMRd lesions. An RNA-based classification of the immune-infiltration identified clusters polarized for yH2AX accumulation, mainly associated with specific relative and qualitative TILs content and differential clinical behaviour.

Two major topics emerge from the yH2AX staining results across different cancer types. First, the discrepancy of the scoring system across different reports affects a reliable comparison.^{21,28,41-44} We recorded intensity and pervasiveness of the yH2AX staining, thus allowing a *post-hoc* binarization of data. Conversely, most of the published results did not consider degrees of expression, usually comparing pathological data between positive (high expressors) and negative (not high expressors) tumors.^{21,41,43,44} This scenario influences comparisons in terms of prevalence of yH2AX positivity across studies. Breast tumors showed a 30% positivity rate for yH2AX,⁴⁵ more prevalent in triple negative lesions.⁴⁶ A quarter of the early-stage lung carcinomas²¹ showed high yH2AX staining, whereas all the gastric cancers analyzed by Guo et al. showed a detectable level of staining.⁴³ In a study focused on 92, all stages CRCs, Lee and colleagues developed a 3-level system, in which the yH2AX grade II and III, representing the positive lesions, led to a 61% positivity rate. Although slightly lower, this prevalence is in line with our data (positivity rate of 78%): indeed, grade I by Lee and colleagues (negative for yH2AX) also contained lesions with weak accumulation, thus explaining this minimal misalignment.²⁸

In our study we correlated yH2AX expression levels to pathological features routinely recorded in clinical practice that help prognostically stratify CRC patients. Less differentiated lesions showed higher yH2AX expression levels and yH2AX accumulation correlated with tumor budding: about 90% of Bd2 and Bd3 CRCs expressed yH2AX, whereas 40% of Bd0 and Bd1 lesions lacked yH2AX expression. The only report assessing tumor budding is related to cervical cancer and confirmed a higher yH2AX accumulation in the cells at the invasive front of the tumor, suggesting a potential role for yH2AX as sensor for tumor invasion.⁴⁴ Furthermore, in our cohort MMRd lesions showed a higher prevalence of yH2AX negative tumors (36% vs 18% of MMRp). The other CRC study on record did not assess this feature, and no data on a potential relationship between loss of MMR and the level of phosphorylation of yH2AX are on record.^{47,48}

The second part of the study was triggered by 2 assumptions: (1) CRCs are conceptually classified as “hot” or “cold” by the extent of the infiltrating immune-cell microenvironment and the response to immune-therapies;^{49,50} (2) in “hot” lesions the recruitment of the immune cells is generally triggered by neoantigens produced by an accumulation of DNA alterations not repaired in a MMR deficiency scenario. A recent review reported a correlation between DSBs and the inception of an immune-fertile tumor infiltrate;²⁷ hence, we wondered if a marker of

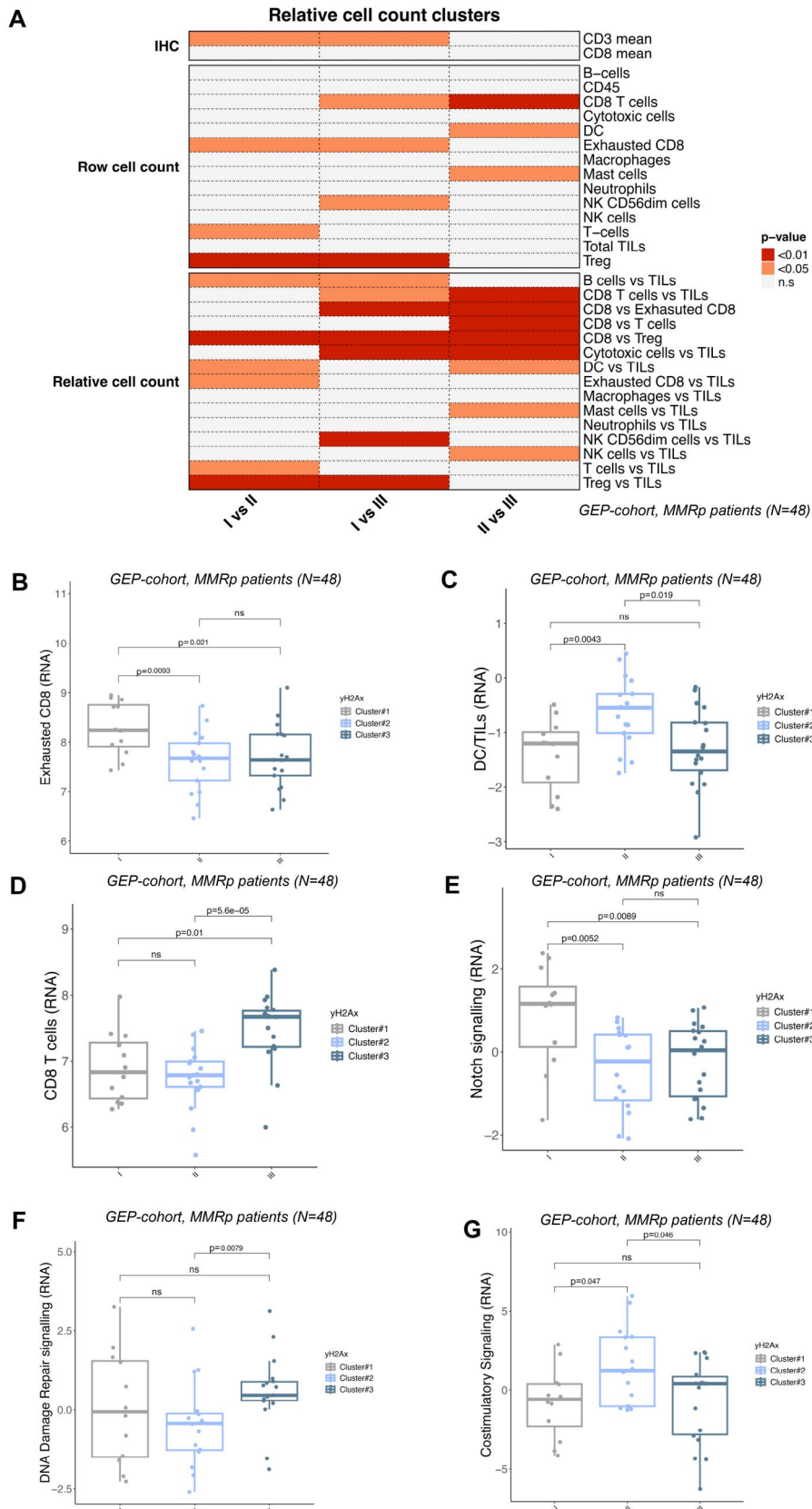


Figure 4. Correlation between the *k*-mean clusters, the immune microenvironment and the pathway activation inferred by the gene expression profiling. (A) Heatmap of the *P*-value reporting the significant comparisons between the immune clusters. (B) Boxplot of exhausted CD8 distribution within the immune clusters. (C) Boxplot of dendritic cell (DC)/TILs distribution within the immune clusters. (D) Boxplot of CD8 distribution within the immune clusters. (E) Boxplot of Notch signaling score within the immune clusters. (F) Boxplot of DNA damage repair signaling score within the immune clusters. (G) Boxplot of costimulatory signaling score within the immune clusters.

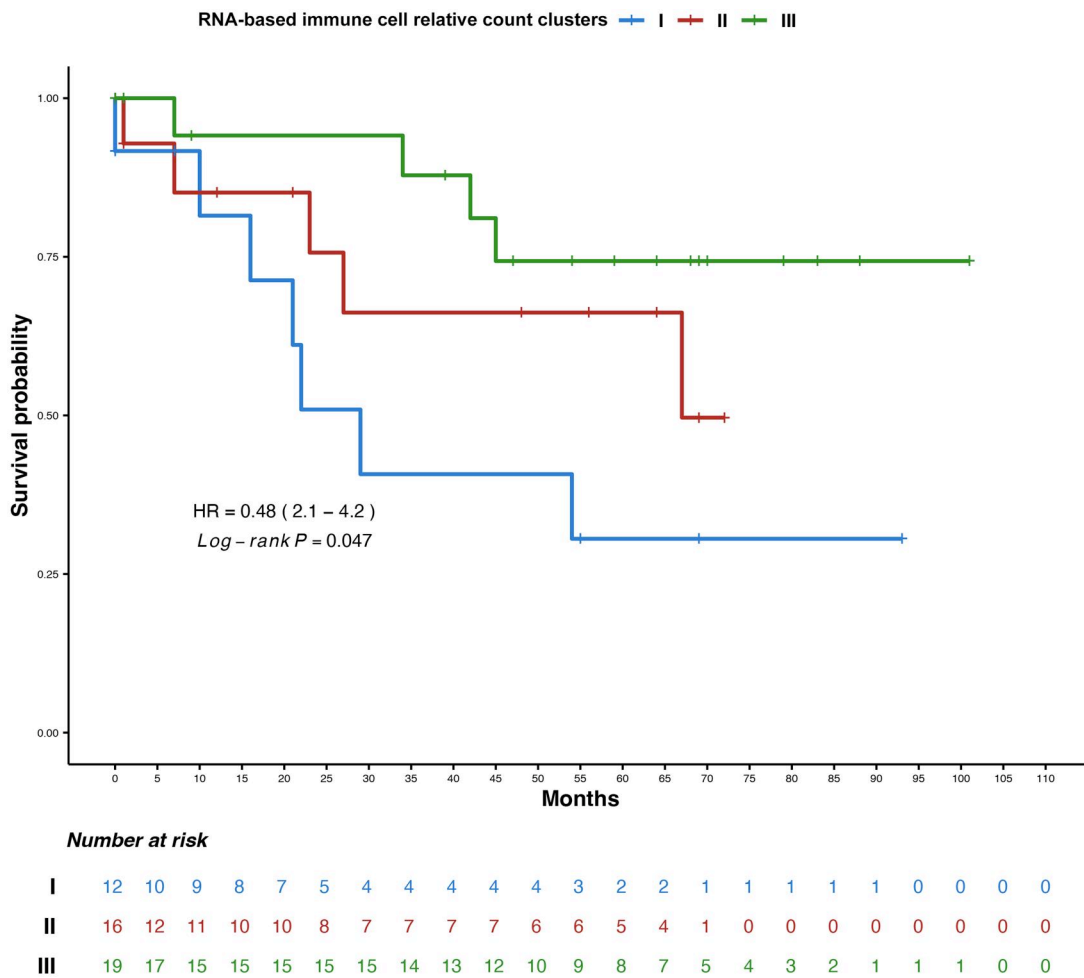


Figure 5. Overall survival Kaplan–Meier curves with HR and *P*-value for the relative cell count immune related clusters in the MMR proficient cohort analyzed for the gene expression profiling.

DBSs (γH2AX) was associated to a specific immune cell type microenvironment.

Since MMRd tumors, less positive and usually immune-inflamed, represented a potential confounder for stratification, we focused on MMRp lesions, and we observed that relative quality rather than the quantity clustered and correlated with γH2AX accumulation. Recently, MSS lesions have been distinguished in 2 immune-related groups: the type II, like MSI lesions for the immune infiltration, characterized by increased CD8+ and Tregs, and the type I, characterized by a large extend of M2 macrophages and a higher proportion of B-cells.⁵¹

In our hands, the relative amount of each immune cell-type inferred by RNA profiling identified 3 groups. Cluster#1, mainly composed by MMRp/γH2AX⁻ lesions, characterized by an increase of B-cells and an enrichment of exhausted CD8⁺ T cells, a hallmark of cancer immune evasion in MMRp CRCs.⁵² Clusters #2 and #3, enriched in γH2AX⁺ CRCs, differed from each other for CD8+ T-cells, and both showed a greater raw and relative count of Tregs compared to the Cluster #1. In this scenario, although higher amount of CD8+ T-cells are proper of MSI favorable CRCs,⁵³ recent single-cell analysis demonstrated that MSS/CD8⁺ T-cell high lesions show a low diversity of the TCR, leading to a group of CRCs less “immunogenic” than expected.⁵⁴

Importantly, the 2 γH2AX-positive MMRp clusters were not redundant but reflected distinct immune configurations: Cluster #2 was enriched in dendritic cells and costimulatory signalling, consistent with an antigen-presentation/priming-oriented milieu. This suggests an immune context driven by antigen processing and T-cell priming rather than effector dominance. In contrast, cluster #3 showed a stronger CD8+ T-cell component with a prominent DDR program, indicating a more effector-oriented landscape linked to sustained DNA damage signalling. Notably, in MSS CRC, CD8-high states may also reflect bystander (“pseudo-hot”) activation rather than fully tumor-reactive immunity. Therefore, while both clusters are γH2AX-positive, cluster #2 appears to define a priming/costimulatory axis of immune engagement, whereas cluster #3 reflects a cytotoxic/DDR-associated axis, underscoring the heterogeneity of γH2AX-positive MMRp tumors.^{55–57}

Finally, we exploratory evaluated γH2AX as a prognostic biomarker. In the entire population multivariate analysis revealed a 1.5-fold (but not significant) HR for γH2AX-positive lesions, which confirms a previously reported trend in a mixed cohort of early and advanced CRCs.²⁸ A different scenario was encountered considering the γH2AX-immune related clusters: the γH2AX-negative group showed the worst survival, whereas

cluster III (γ H2AX⁺, CD8⁺ and Treg high) displayed the best outcome overall, with a 0.17-fold HR compared to cluster I. Although preliminary, this observation may suggest that a subset of γ H2AX-positive MMRp tumors shares selected immune and clinical features with MSI/MMRd CRC; however, the heterogeneity observed within γ H2AX-positive cases indicates that additional immune-contexture characteristics contribute to this stratification.

The main limitation of the study is related to the retrospective nature of the cohort, affecting both the choice of a targeted gene expression profiling method and the clinical data collection. The archival samples available led to perform transcriptomic analyses on a technically feasible subset rather than the entire cohort. Nevertheless, the analyzed subset remained highly representative of the overall cohort in terms of clinico-pathological characteristics and γ H2AX distribution.

Finally, when considering survival data, the prognostic role of our biomarkers could have been influenced by the heterogeneity in patient management.

In conclusion, the assessment of γ H2AX accumulation, as a proxy of DSBs, identifies a subset of MSS CRCs characterized by distinct immune configurations. Within γ H2AX-positive MMRp tumors, heterogeneous immune patterns emerge, including a subgroup displaying immune and clinical features partially overlapping with those observed in MSI/MMRd CRC. γ H2AX may contribute to refine the immunobiological stratification of MSS CRCs rather than serving as a standalone surrogate of MSI-like behavior. Further clinical validation in homogeneously treated cohorts is warranted.

Acknowledgments

We are grateful to individuals who took part in the Alpha-Omega Program and generously consented access to tumor samples, thereby contributing to the advancement of this research. We would like to thank the technical and medical staff of the Pathology Unit of FPO-IRCCS Candiolo Cancer Institute and Ospedale Niguarda for support in tissue sample processing and handling for molecular downstream analyses.

Author contributions

Enrico Berrino (Conceptualization, Data curation, Formal analysis, Investigation, Methodology, Supervision, Validation, Visualization, Writing—original draft, Writing—review & editing), Sara Erika Bellomo (Data curation, Funding acquisition, Investigation, Methodology, Software, Writing—original draft), Maria Costanza Aquilano (Conceptualization, Data curation), Marta Falcinelli (Conceptualization, Data curation, Writing—review & editing), Anita Chesta (Data curation, Writing—review & editing), Emanuele Valtorta (Investigation, Methodology), Daniela Zampieri (Investigation, Methodology), Gianluca Mauri (Investigation, Methodology, Writing—review & editing), Giuseppe Sala (Investigation, Methodology), Silvia Marsoni (Investigation, Methodology), Alberto Bardelli (Investigation, Methodology), Andrea Sartore-Bianchi (Investigation, Methodology), Salvatore Siena (Investigation, Methodology), Anna Sapino (Writing—review & editing), Emanuela Bonoldi

(Methodology), Fabrizio d'Adda di Fagagna (Conceptualization, Data curation, Methodology, Writing—original draft, Writing—review & editing), and Caterina Marchiò (Conceptualization, Data curation, Investigation, Methodology, Writing—review & editing)

Supplementary material

Supplementary material is available at *The Oncologist* online

Funding

This work was supported by FONDAZIONE AIRC (Associazione Italiana per la Ricerca sul Cancro) under 5 per Mille 2018—ID 21091 program—PI: A.b., group leaders C.M. and FdADF; Fondazione Piemontese per la Ricerca sul Cancro-ONLUS, 5x1000 Ministero della Salute 2022, grant CARESS (to C.M.); and the Italian Ministry of Health Ricerca Corrente 2024-2025. Study materials were also supported by Fondo Divisionale Oncologia Falck, Grande Ospedale Metroplitano Niguarda, and by Fondazione Oncologia Niguarda ETS. FdADF group is supported by: ERC advanced grant TELORNAGING—835103, ERC POC TELOVACCINE—101113229, AIRC-IG 30471, AIRC-IG 21762., Telethon GMR23T2007, Progetti di Ricerca di Interesse Nazionale (PRIN) 2020CXFL4T, Progetti di Ricerca di Interesse Nazionale (PRIN) 2022R7LH5T, AriSLA DDR&ALS FG_24_2020, POR FESR InterSLA DSB.AD004.294, Next Generation EU, in the context of the National Recovery and Resilience Plan, Investment PE8 Project Age-It. Investment CN3 National Center for Gene Therapy and Drugs based on RNA Technology. In addition, we would like to acknowledge that the research leading to these results has received funding from: European Research Council (ERC) under the European Union's Horizon 2020 research and innovation programme (TARGET, grant agreement n. 101020342) (A.B.); IMI contract n. 101007937 PERSIST-SEQ (A.B.); AIRC under IG 2023 - ID. 289ASSO22 project—P.I. Bardelli Alberto (A.B.). Views and opinions expressed are however those of the author(s) only and do not necessarily reflect those of the European Union or the European Research Council. Neither the European Union nor the granting authority can be held responsible for them.

Submission declaration and verification

The present manuscript was not previously published or under consideration elsewhere. We presented these preliminary results as poster at the 2025 USCAP congress (DOI: 10.1016/j.labinv.2024.102794)

Conflicts of interest

A.B. reports receipt of grants/research supports from Neophore, is a stock shareholder of Neophore and Kither Biotech, and is an advisory board member for Neophore. C.M. reports personal consultancy fees from Bayer, Roche, Menarini, Astrazeneca and Illumina outside the scope of the present work. S.M. reports the following financial relationships: University of Chicago

(Speaker), EORTC Traveling/Accommodation to twice a year Brussels Meeting IDMC (Independent Data Monitoring Committee) Member, Fondazione Tempia Biella Traveling Expenses Permanent SAB Member. FdAdF is a co-founder and shareholder of TAG Therapeutics. G.M. reports speaker honoraria from Amgen. The other authors declare no COIs.

Data availability

This study includes no data deposited in external repositories. Source data and Extended Data files are provided with this paper. All other data supporting the findings of this study are available from the corresponding author on reasonable request.

References

1. Yao Y, Dai W. Genomic instability and cancer. *J Carcinog Mutagen*. 2014;5:1–17. <https://doi.org/10.4172/2157-2518.1000165>.
2. Ferguson LR, Chen H, Collins AR, et al. Genomic instability in human cancer: molecular insights and opportunities for therapeutic attack and prevention through diet and nutrition. *Semin Cancer Biol*. 2015;35 Suppl:S5-S24. <https://doi.org/10.1016/j.semcancer.2015.03.005>.
3. Helleday T, Petermann E, Lundin C, Hodgson B, Sharma RA. DNA repair pathways as targets for cancer therapy. *Nat Rev Cancer*. 2008;8:193-204. <https://doi.org/10.1038/nrc2342>.
4. Kanev PB, Ateamin A, Stoyanov S, Aleksandrov R. PARP1 roles in DNA repair and DNA replication: the basi(c)s of PARP inhibitor efficacy and resistance. *Semin Oncol*. 2024;51:2-18. <https://doi.org/10.1053/j.seminoncol.2023.08.001>.
5. Wiegman AP, Ward A, Ivanova E, et al. Genome instability and pressure on non-homologous end joining drives chemotherapy resistance via a DNA repair crisis switch in triple negative breast cancer. *NAR Cancer*. 2021;3:zcab022. <https://doi.org/10.1093/narcan/zcab022>.
6. Woo SM, Kim MK, Park B, et al. Genomic instability of circulating tumor DNA as a prognostic marker for pancreatic cancer survival: a prospective cohort study. *Cancers (Basel)*. 2021;13: <https://doi.org/10.3390/cancers13215466>.
7. Hosea R, Hillary S, Naqvi S, Wu S, Kasim V. The two sides of chromosomal instability: drivers and brakes in cancer. *Signal Transduct Target Ther*. 2024;9:75. <https://doi.org/10.1038/s41392-024-01767-7>.
8. Brown JS, O’Carrigan B, Jackson SP, Yap TA. Targeting DNA repair in cancer: beyond PARP inhibitors. *Cancer Discov*. 2017;7:20-37. <https://doi.org/10.1158/2159-8290.CD-16-0860>.
9. Bartek J. DNA damage response, genetic instability and cancer: from mechanistic insights to personalized treatment. *Mol Oncol*. 2011;5:303-307. <https://doi.org/10.1016/j.molonc.2011.07.006>.
10. Li Q, Qian W, Zhang Y, Hu L, Chen S, Xia Y. A new wave of innovations within the DNA damage response. *Signal Transduct Target Ther*. 2023;8:338. <https://doi.org/10.1038/s41392-023-01548-8>.
11. Jeggo PA, Pearl LH, Carr AM. DNA repair, genome stability and cancer: a historical perspective. *Nat Rev Cancer*. 2016;16:35-42. <https://doi.org/10.1038/nrc.2015.4>.
12. Di Micco R, Fumagalli M, d’Adda di Fagagna F. Breaking news: high-speed race ends in arrest—how oncogenes induce senescence. *Trends Cell Biol*. 2007;17:529-536. <https://doi.org/10.1016/j.tcb.2007.07.012>.
13. Swift LH, Golsteyn RM. Genotoxic anti-cancer agents and their relationship to DNA damage, mitosis, and checkpoint adaptation in proliferating cancer cells. *Int J Mol Sci*. 2014;15:3403-3431. <https://doi.org/10.3390/ijms15033403>.
14. Vignard J, Mirey G, Salles B. Ionizing-radiation induced DNA double-strand breaks: a direct and indirect lighting up. *Radiother Oncol*. 2013;108:362-369. <https://doi.org/10.1016/j.radonc.2013.06.013>.
15. Khanna KK, Jackson SP. DNA double-strand breaks: signaling, repair and the cancer connection. *Nat Genet*. 2001;27:247-254. <https://doi.org/10.1038/85798>.
16. Gillyard T, Davis J. DNA double-strand break repair in cancer: a path to achieving precision medicine. *Int Rev Cell Mol Biol*. 2021;364:111-137. <https://doi.org/10.1016/bs.ircmb.2021.06.003>.
17. Aparicio T, Baer R, Gautier J. DNA double-strand break repair pathway choice and cancer. *DNA Repair (Amst)*. 2014;19:169-175. <https://doi.org/10.1016/j.dnarep.2014.03.014>.
18. Kinner A, Wu W, Staudt C, Iliakis G. Gamma-H2AX in recognition and signaling of DNA double-strand breaks in the context of chromatin. *Nucleic Acids Res*. 2008;36:5678-5694. <https://doi.org/10.1093/nar/gkn550>.
19. Collins PL, Purman C, Porter SI, et al. DNA double-strand breaks induce H2AX phosphorylation domains in a contact-dependent manner. *Nat Commun*. 2020;11:3158. <https://doi.org/10.1038/s41467-020-16926-x>.
20. Kuo LJ, Yang LX. Gamma-H2AX - a novel biomarker for DNA double-strand breaks. *In Vivo*. 2008;22:305-309.
21. Matthaïos D, Foukas PG, Kefala M, et al. gamma-H2AX expression detected by immunohistochemistry correlates with prognosis in early operable non-small cell lung cancer. *Onco Targets Ther*. 2012;5:309-314. <https://doi.org/10.2147/OTT.S36995>.
22. Sone M, Toyoda T, Cho YM, et al. Immunohistochemistry of gamma-H2AX as a method of early detection of urinary bladder carcinogenicity in mice. *J Appl Toxicol*. 2019;39:868-876. <https://doi.org/10.1002/jat.3775>.
23. Brunner AH, Hinterholzer S, Riss P, Heinze G, Weiss K, Brustmann H. Expression of gamma-H2AX in endometrial carcinomas: an immunohistochemical study with p53. *Gynecol Oncol*. 2011;121:206-211. <https://doi.org/10.1016/j.ygyno.2010.11.037>.
24. Kawashima S, Kawaguchi N, Taniguchi K, et al. gamma-H2AX as a potential indicator of radiosensitivity in colorectal cancer cells. *Oncol Lett*. 2020;20:2331-2337. <https://doi.org/10.3892/ol.2020.11788>.
25. Knipper K, Hussein Y, Simon AG, et al. Upregulation of the histone gamma-H2AX correlates with worse patient survival and basal-like subtype in pancreatic ductal adenocarcinoma. *J Cancer Res Clin Oncol*. 2024;150:137. <https://doi.org/10.1007/s00432-024-05681-x>.
26. Contreras L, Garcia-Gaipo L, Casar B, Gandarillas A. DNA damage signalling histone H2AX is required for tumour growth. *Cell Death Discov*. 2024;10:99. <https://doi.org/10.1038/s41420-024-01869-9>.

27. Amodio V, Vitiello PP, Bardelli A, Germano G. DNA repair-dependent immunogenic liabilities in colorectal cancer: opportunities from errors. *Br J Cancer*. 2024;131:1576-1590. <https://doi.org/10.1038/s41416-024-02848-8>.
28. Lee YC, Yin TC, Chen YT, et al. High expression of phospho-H2AX predicts a poor prognosis in colorectal cancer. *Anticancer Res*. 2015;35:2447-2453.
29. Germano G, Amirouchene-Angelozzi N, Rospo G, Bardelli A. The clinical impact of the genomic landscape of mismatch repair-deficient cancers. *Cancer Discov*. 2018;8:1518-1528. <https://doi.org/10.1158/2159-8290.CD-18-0150>.
30. Amodio V, Mauri G, Reilly NM, et al. Mechanisms of immune escape and resistance to checkpoint inhibitor therapies in mismatch repair deficient metastatic colorectal cancers. *Cancers (Basel)*. 2021;13: <https://doi.org/10.3390/cancers13112638>.
31. Germano G, Lamba S, Rospo G, et al. Inactivation of DNA repair triggers neoantigen generation and impairs tumour growth. *Nature*. 2017;552:116-120. <https://doi.org/10.1038/nature24673>.
32. Kim JK, Chen CT, Keshinro A, et al. Intratumoral T-cell repertoires in DNA mismatch repair-proficient and -deficient colon tumors containing high or low numbers of tumor-infiltrating lymphocytes. *Oncoimmunology*. 2022;11:2054757. <https://doi.org/10.1080/2162402X.2022.2054757>.
33. Yang B, Rao W, Luo H, Zhang L, Wang D. Relapse-related molecular signature in early-stage lung adenocarcinomas based on base excision repair, stimulator of interferon genes pathway and tumor-infiltrating lymphocytes. *Cancer Sci*. 2020; 111:3493-3502. <https://doi.org/10.1111/cas.14570>.
34. Voutilainen S, Heikkilä P, Bartkova J, et al. Markers associated with genomic instability, immunogenicity and immune therapy responsiveness in metaplastic carcinoma of the breast: expression of gammaH2AX, pRPA2, P53, PD-L1 and tumor infiltrating lymphocytes in 76 cases. *BMC Cancer*. 2022;22:1298. <https://doi.org/10.1186/s12885-022-10408-7>.
35. Berrino E, Aquilano MC, Valtorta E, et al. Unique patterns of heterogeneous mismatch repair protein expression in colorectal cancer unveil different degrees of tumor mutational burden and distinct tumor microenvironment features. *Mod Pathol*. 2023;36:100012. <https://doi.org/10.1016/j.modpat.2022.100012>.
36. Wensink GE, Elias SG, Mullenders J, et al. Patient-derived organoids as a predictive biomarker for treatment response in cancer patients. *NPJ Precis Oncol*. 2021;5:30. <https://doi.org/10.1038/s41698-021-00168-1>.
37. Verduin M, Hoeben A, De Ruysscher D, Vooijs M. Patient-derived cancer organoids as predictors of treatment response. *Front Oncol*. 2021;11:641980. <https://doi.org/10.3389/fonc.2021.641980>.
38. Tong L, Cui W, Zhang B, et al. Patient-derived organoids in precision cancer medicine. *Med*. 2024;5:1351-1377. <https://doi.org/10.1016/j.medj.2024.08.010>.
39. Sun D, Gao W, Hu H, Zhou S. Why 90% of clinical drug development fails and how to improve it? *Acta Pharm Sin B*. 2022; 12:3049-3062. <https://doi.org/10.1016/j.apsb.2022.02.002>.
40. Khalil AS, Jaenisch R, Mooney DJ. Engineered tissues and strategies to overcome challenges in drug development. *Adv Drug Deliv Rev*. 2020;158:116-139. <https://doi.org/10.1016/j.addr.2020.09.012>.
41. Wang B, Zhang Z, Xia S, Jiang M, Wang Y. Expression of gamma-H2AX and patient prognosis in breast cancer cohort. *J Cell Biochem*. 2019;120:12958-12965. <https://doi.org/10.1002/jcb.28567>.
42. Katsuta E, Sawant Dessai A, Ebos JM, Yan L, Ouchi T, Takabe K. H2AX mRNA expression reflects DNA repair, cell proliferation, metastasis, and worse survival in breast cancer. *Am J Cancer Res*. 2022;12:793-804.
43. Guo Z, Pei S, Si T, et al. Expression of the gamma-phosphorylated histone H2AX in gastric carcinoma and gastric precancerous lesions. *Oncol Lett*. 2015;9:1790-1794. <https://doi.org/10.3892/ol.2015.2896>.
44. Shang L, Li X, Song Y, Zhao J, Guo Z. The role of γ H2AX and H2AX in cervical carcinogenesis, invasion, and metastasis, and their relationship with the expression of E-cadherin. *Eur J Gynaecol Oncol*. 2025;46:16-26. <https://doi.org/10.22514/ejgo.2025.032>.
45. Yang SX, Polley EC, Nguyen D. Association of gammaH2AX at diagnosis with chemotherapy outcome in patients with breast cancer. *Theranostics*. 2017;7:945-951. <https://doi.org/10.7150/thno.19102>.
46. Nagelkerke A, van Kuijk SJ, Sweep FC, et al. Constitutive expression of gamma-H2AX has prognostic relevance in triple negative breast cancer. *Radiother Oncol*. 2011;101:39-45. <https://doi.org/10.1016/j.radonc.2011.07.009>.
47. Wu CY, Kang HY, Yang WL, et al. Critical role of monoubiquitination of histone H2AX protein in histone H2AX phosphorylation and DNA damage response. *J Biol Chem*. 2011;286: 30806-30815. <https://doi.org/10.1074/jbc.M111.257469>.
48. Sawant A, Kothandapani A, Zhitkovich A, Sobol RW, Patrick SM. Role of mismatch repair proteins in the processing of cisplatin interstrand cross-links. *DNA Repair (Amst)*. 2015;35:126-136. <https://doi.org/10.1016/j.dnarep.2015.10.003>.
49. Liu JL, Yang M, Bai JG, Liu Z, Wang XS. "Cold" colorectal cancer faces a bottleneck in immunotherapy. *World J Gastrointest Oncol*. 2023;15:240-250. <https://doi.org/10.4251/wjgo.v15.i2.240>.
50. Wu B, Zhang B, Li B, Wu H, Jiang M. Cold and hot tumors: from molecular mechanisms to targeted therapy. *Signal Transduct Target Ther*. 2024;9:274. <https://doi.org/10.1038/s41392-024-01979-x>.
51. Esposito A, Agostini A, Quero G, et al. Colorectal cancer patients-derived immunity-organoid platform unveils cancer-specific tissue markers associated with immunotherapy resistance. *Cell Death Dis*. 2024;15:878. <https://doi.org/10.1038/s41419-024-07266-5>.
52. Jiang Y, Li Y, Zhu B. T-cell exhaustion in the tumor microenvironment. *Cell Death Dis*. 2015;6:e1792. <https://doi.org/10.1038/cddis.2015.162>.
53. Toh JWT, Ferguson AL, Spring KJ, Mahajan H, Palendira U. Cytotoxic CD8+ T cells and tissue resident memory cells in colorectal cancer based on microsatellite instability and BRAF status. *World J Clin Oncol*. 2021;12:238-248. <https://doi.org/10.5306/wjco.v12.i4.238>.
54. Borrás DM, Verbandt S, Ausserhofer M, et al. Single cell dynamics of tumor specificity vs bystander activity in CD8(+) T

- cells define the diverse immune landscapes in colorectal cancer. *Cell Discov.* 2023;9:114. <https://doi.org/10.1038/s41421-023-00605-4>.
55. Bauer K, Nelius N, Reuschenbach M, et al. T cell responses against microsatellite instability-induced frameshift peptides and influence of regulatory T cells in colorectal cancer. *Cancer Immunol Immunother.* 2013;62:27-37. <https://doi.org/10.1007/s00262-012-1303-8>.
56. Kim KJ, Lee KS, Cho HJ, et al. Prognostic implications of tumor-infiltrating FoxP3+ regulatory T cells and CD8+ cytotoxic T cells in microsatellite-unstable gastric cancers. *Hum Pathol.* 2014;45:285-293. <https://doi.org/10.1016/j.humpath.2013.09.004>.
57. Michel S, Benner A, Tariverdian M, et al. High density of FOXP3-positive T cells infiltrating colorectal cancers with microsatellite instability. *Br J Cancer.* 2008;99:1867-1873. <https://doi.org/10.1038/sj.bjc.6604756>.